Effects of flow volume and grain size on mobility of dry granular flows of angular rock fragments: A functional relationship of scaling parameters

B. Cagnoli[1] and G.P. Romano[2]

[1]Istituto Nazionale di Geofisica e Vulcanologia, Via di Vigna Murata 605, 00143 Rome, Italy.

[2]Department of Mechanical and Aerospace Engineering, La Sapienza University, Via Eudossiana 18, 00184 Rome, Italy.

[1] Flows of angular rock fragments are released down a concave upward chute in the laboratory to study their mobility. This mobility is measured as the reciprocal of the apparent coefficient of friction that is equal to the vertical drop of the centre of mass of the granular material divided by its horizontal distance of travel. Our experiments show that the finer the grain size (all the other features the same), the larger is the mobility of the centre of mass. We believe this to be due to the fact that in finer grain size flows there are less agitated particles per unit of flow mass so that these flows dissipate less energy per unit of travel distance. Our experiments show also that the larger the volume (all the other features the same), the larger is the apparent coefficient of friction. We believe this to be so because the frontal portion of a flow reaches the less steep part of a curved slope and stops before the rear portion preventing the rear portion and the centre of mass from travelling further downhill. This phenomenon (which is more prominent in larger volume flows whose rear and frontal ends are more distant) counteracts the decrease of energy dissipation per unit of flow mass, due to the decrease of particle agitation per unit of flow mass, that is expected when the volume of a flow increases (all the other features the same). Our analysis generates a functional relationship between the dimensionless apparent coefficient of friction and a scaling parameter whose numerator is equal to the mean grain size multiplied by the cube root of the deposit volume and whose denominator is the square of the channel width.

Citation: Cagnoli, B., and G.P. Romano (….), Effects of flow volume and grain size on mobility of dry granular flows of angular rock fragments: A functional relationship of scaling parameters, *J. Geophys. Res.*, …

1. Introduction

[2] In this paper we investigate experimentally the effect that increasing the volume of flows with the same or different grain size has on the final position of the centre of mass of their deposits. Ours are dry granular flows of angular rock fragments that travel within a channel on a concave upward slope. These experiments are relevant for the understanding of the mobility of pyroclastic flows and rock avalanches [*Cas and Wright*, 1988; *Pudasaini and Hutter*, 2006] whose study is important to assess natural hazards in mountain regions.

[3] Our dense laboratory flows are meant to reproduce the high-density, basal part of pyroclastic flows that consists of a narrow, long tongue of rock debris [e.g., *Nairn and Self*, 1978; *Rowley et al.*, 1981; *Saucedo et al.*, 2004; *Lube et al.*, 2007]. The deposits of the basal part are internally structureless (i.e., massive) and poorly sorted but they sometimes show a vertical coarse-tail grading that can be normal (coarser grains down) or reverse (coarser grains up) [*Cagnoli et al.*, 1994; *Cagnoli and Manga*, 2005]. These pyroclastic flows have also an overriding ash cloud, but this turbulent cloud (that can move independently) requires experiments different from those described here to be studied [e.g., *Dellino et al.*, 2007]. Our flows are dry and for this reason they can simulate also rock avalanches which differ from the so-called lahars and debris flows that are characterized by the presence of intergranular water and mud [e.g., *McArdell et al.*, 2007]. Here, we deal with granular masses that after an initial internal deformation (that corresponds to slope or volcanic dome failures) acquire a distinct mature shape of travel moving within a channel. This differs from studies of cliff and granular column collapses that are dominated by the initial internal deformation and where most of the granular mass propagates on a layer of already deposited grain

[e.g., *Lucas and Mangeney*, 2007; *Lube et al.*, 2011]. Our flows of angular rock fragments are also unsteady and, for this reason, their behaviour is expected to be different from that of steady flows of glass beads [e.g., *Jop et al.*, 2006] where glass beads and rock fragments have significantly different properties. We are also interested in the actual energy dissipation due to particle-particle and particle-boundary interactions. This is different from the approach that considers the granular mass as a continuum [e.g., *Savage and Hutter*, 1989].

[4] We use the same experimental apparatus we have used to obtain the results described in two previous publications [*Cagnoli and Romano*, 2010a, 2010b]. In these earlier works we demonstrated that the finer the grain size (all the other features the same), the more mobile is the centre of mass of the flows. This is due to the fact that, the finer the grain size, the less agitated are the rock fragments per unit of flow mass so that finer grain size flows dissipate less energy per unit of travel distance [*Cagnoli and Romano,* 2010a]. Particles are less agitated per unit of flow mass, because, in finer grain size flows (all the other features equal), there is a larger number of rock fragments and, for this reason, the agitation due to the interaction with the rough sidewalls penetrates relatively less inside the flows (Figure 1) as shown by high speed video camera images [*Cagnoli and Romano,* 2010a]. In our previous works, we measured particle agitation by computing the normalised average squared deviation from the mean of the particle transversal speeds where normalisation is by the square of the longitudinal flow speed. The value of this parameter for 30 g flows with a 2-3 mm grain size is ~2.5 times larger than that for 30 g flows with a 0.5-1 mm grain size [*Cagnoli and Romano,* 2010a]. Particle agitation affects energy dissipation through particle-particle and particle-boundary interactions (friction and collisions) and through diversion of energy into directions (the transversal one for example) that are different from the downslope direction.

[5] We obtained also a relationship between the normalised average deviation from the mean of the pressure exerted on a load cell at the base of the flows and a parameter containing grain size and flow volume [*Cagnoli and Romano*, 2010b]. The normalised pressure deviation represents a normalised particle agitation and it can be interpreted as the reciprocal of a potential mobility of the

flow, i.e., its intrinsic ability, at the grain scale, to dissipate more energy or less energy in one single spot on the chute (where the load cell is located for example) [*Cagnoli and Romano*, 2010b]. The load cell reveals that particle collisions affect importantly the interaction of granular flows of rock fragments with the containing (lateral and basal) surfaces. Such a variable basal pressure suggests that the use of Coulomb's law [*Savage and Hutter*, 1989] when modelling granular flows refers to time-averaged values of normal and shear stresses instead of the actual ones that vary significantly during flow motion.

[6] The potential mobility increases as particle agitation per unit of flow mass decreases because, in this case, the flow dissipates less energy per unit of travel distance. Particle agitation per unit of flow mass decreases as grain size decreases or as flow volume increases (all the other features the same) because in both cases (Figure 1) there is a larger number of particles in the flow and the agitation due to the interaction with the rough sidewalls penetrates relatively less inside the flow [*Cagnoli and Romano*, 2010a]. However, the potential mobility does not suffice to predict the final position of the centre of mass of the deposits. For example, it implies that flow mobility increases as grain size decreases or as flow volume increases. But, although our experiments do show this effect of grain size, this effect of volume is counteracted by other phenomena. In this paper, we study the effect of volume and grain size on the final position of the centre of mass of deposits of granular flows of angular rock fragments travelling within channels on concave upward slopes (such as volcano flanks).

2. Method

[7] The experimental apparatus consists of a straight metallic accelerating ramp and a curved marble chute (Figure 2). The chute is made of marble and it rests on an extremely heavy table to prevent vibrations of the apparatus that can disturb the experiments. Before motion, the granular material is placed behind a sliding gate within the accelerator. The gate is removed manually to start

the experiments. Both ramp and chute have the same trapezoidal cross section (inset in Figure 2) that corresponds, in nature, to a v-shaped topographic incision with sediment infilling in the centre. This cross section contains the flows with sidewall effects that are expected to be smaller than those in channels with a less realistic rectangular cross section where the flows are more constrained laterally [e.g., *Cagnoli and Quareni*, 2009]. The trapezoidal surface of the chute is made of plaster whose roughness is everywhere significantly smaller than the smaller grain size we use. The curved chute is 5.4 cm wide and its horizontal length is 1.4 m (Figure 2).

[8] On the curved chute, the slope-parallel component of the acceleration of gravity decreases gradually downslope allowing the flows to stop. The hyperbolic sine equation of the longitudinal profile,

$$z = 0.3 - 0.085 \operatorname{arcsinh}(11.765\, x)\,, \qquad (1)$$

is a slightly modified version of the profile of Mayon volcano in the Philippines [*Becker*, 1905]. Other concave upward slopes of other volcano flanks are shown, for example, by *Voight and Sousa* [1994] and *Lube et al.* [2007].

[9] We use mixtures of rock fragments with three relatively narrow grain size ranges: 0.5-1, 1-2 and 2-3 mm. These mixtures are obtained by crushing an aphanitic volcanic rock block (density ~ 2700 kg/m^3) and sieving the fragments to select the grain sizes. The fragments are angular (Figure 3) with relatively large angles of internal friction: 61.5±1°, 62±1° and 60.5±1° for increasing grain size respectively. These values are indistinguishable (their error bars overlap) and they compare well with an angle of 60° for angular rock fragments reported by *Holtz and Kovacs* [1981]. These angles are the averages of the results of seven bin-flow tests [*Zenz and Othmer*, 1960] for each grain size. In a bin-flow test, the angle of internal friction is estimated as the angle from the horizontal formed by the lines of demarcation between stationary and moving fragments in a narrow rectangular glass container with a small opening in the centre of the base from where the

particles can fall freely. This angle of internal friction is different in meaning and value from the angle of repose [*Zenz and Othmer*, 1960]. Also the intrinsic bounciness (i.e., the coefficient of restitution) of the rock material does not differ among our fragments because they are made of the same rock material. Here, we refer to the bounciness as a function of the material alone which is different from the bounciness measured in collisions with random impact angles of irregularly-shaped fragments whose value is significantly scattered [*Cagnoli and Manga*, 2003]. This is so because the outcome of a particle collision depends on numerous variables [*Goldsmith*, 2001], such as grain size and particle shape, which are already considered individually in the dimensional analysis. The scatter due to different impact angles and irregular particle shapes can be prevented measuring the vertical rebound of a sphere made of the material of interest after impacts on a flat and horizontal surface of a rigid body made of the same or a different material.

[10] The main set of experiments is carried out by loading the accelerator with samples of two different masses (30 and 60 g) for each grain size. These samples are released from behind a gate that is always located 22.3 cm above x=0 where this distance is measured along the accelerator (Figure 2). Each experiment with its specific characteristics is repeated five times to assess the repeatability. Each time we use a different batch of granular material with the same characteristics. The purpose of the main set of experiments is to study the effect of flow volume and grain size on the final position of the centre of mass of the deposits.

[11] In these experiments, only grain size and flow volume change. The values of all the other variables that can affect the flow mobility are constant. In particular, angle of internal friction, coefficient of restitution and density of these same-rock fragments are the same and the geometric properties (form, angularity and surface texture) of the fragments are also not significantly different (Figure 3). For example, flows of glass beads would have had significantly different mobility because of their properties, such as coefficient of restitution and particles shape, which differ substantially from those of rock fragments [e.g., *Banton et al.*, 2009]. Moreover, the roughness of the chute inner surfaces does not change during our experimental session (as explained later in the

paper) and the shape of the chute longitudinal profile (i.e., its curvature) is also always the same. Furthermore, all our flows have the same temperature (i.e., room temperature). As far as pyroclastic flows are concerned, experiments seem to show that the high temperature alone of rock fragments does not affect the mobility of dense flows in the laboratory [*Takahashi and Tsujimoto*, 2000]. Our experiments are run in a controlled environment where the average relative air humidity is approximately 45% at 22ºC.

[12] Three-dimensional computer representations of all deposits are obtained assessing the position of selected points of their surfaces from photos and laboratory measurements following the procedure adopted by *Cagnoli and Romano* [2010a]. The generated volumes enable the determination of the position in space of the centre of mass of the deposits using CAD software. The same procedure is adopted to locate in space the centre of mass of the granular samples at rest behind the gate (Figure 2). Here we assume that these still granular masses have densities that are virtually uniform in space. In this paper, we measure the distance between the centre of mass of the deposit and the centre of mass of the granular material behind the gate (where the initial velocities of all flows are zero) to establish which flow is more mobile.

3. Features of flows and deposits

[13] Within the accelerating ramp, after the removal of the gate, the granular material deforms into the shape of the flow proper. This deformation consists in the change from the shape the granular material has behind the gate into that of the slug-shaped travelling flows (Figure 4a). Figure 4a shows the mature shape of travel which is the shape the flows have during motion after the initial deformation that occurred in the accelerator and before the final deformation of deposition. The initial deformation corresponds, in nature, to the gravitational collapse of a volcanic dome or a mountain slope (for pyroclastic flows and rock avalanches respectively). Our flows are thus unsteady (also those in nature are unsteady).

[14] In our experiments there is no formation of levees because no granular material is deposited on both sides of the chute during flow motion. Levees are expected in unconfined flows [*Félix and Thomas*, 2004]. Furthermore, no fine powder that can have affected flow mobility is produced by particles during flow motion. Ash produced by mutual abrasion of particles is expected in experiments with softer rock fragments such as pumice fragments [*Cagnoli and Manga*, 2004].

[15] The deposited granular material consists of two portions (Figure 4b and 4c respectively): a more proximal heap that is much more elongated than thick (the deposit of the flow proper) and a more distal distribution of individual fragments [*Cagnoli and Romano,* 2010a]. The distal distribution is formed by fragments, which, bouncing within the chute, travelled individually without interacting and are not part of the flow proper (as shown by high-speed video camera movies). Distal distributions of isolated particles in front of the deposits of the flow proper are common in chute experiments [e.g., *Hutter and Koch*, 1991]. Flows and distal distributions have different movement and deposition mechanisms and they must be considered separately. Here we study only the flows.

[16] The maximum thickness of the deposits is 9±1 mm and 13±1 mm for the 30 and 60 g experiments respectively (where each value is the average of the maximum thicknesses of the deposits with the same mass and the three different grain sizes). These deposits are significantly more extended in length than in thickness (such as those in nature). Figures 5 and 6 and Table 1 illustrate the values of the maximum width and the length (i.e., the longitudinal spreading) of the deposits of the flow proper. These plots show that the finer the grain size, the wider and the shorter the deposits with the same volume tend to be. The positions along the chute of the deposit longitudinal spreadings (length of vertical segments) and the positions of their centres of mass (black circles) are shown in Figure 7 where distances are measured from x=0. Figure 7 and Table 1 show that larger volume deposits (all the other features the same) have a longitudinal spreading that is larger than that of smaller volume deposits. Although the position of the frontal end of the deposits of the flow proper is fuzzy because of the presence of the distal distribution of individual

fragments, here we consider the position of the frontal end of these deposits to be located approximately in the most distal place where the particles are still in contact with one another. This considered, larger volume deposits (all the other features the same) have a frontal end that is in a more distal position than that of smaller volume deposits. This phenomenon is more evident when comparing deposits with more different volumes such as those with masses equal to 30 g and 5 g used in the experiments described in one of our earlier works [*Cagnoli and Romano*, 2010b].

[17] Because the total mass of the granular material at rest behind the gate is equal to the sum of the masses of deposit and distal distribution, the centre of mass of the material behind the gate and that of the deposit alone, in general, cannot be compared. However, for experiments with masses equal to and larger than 30 g, the total mass of the distal distribution of fragments is negligible when compared to that of the deposit of the flow proper [*Cagnoli and Romano*, 2010a]. For this reason, the distal distribution of fragments is not considered here and the position of the centre of mass of the deposits is not affected significantly by the uncertainty in the location of the boundary between deposits and distal distributions.

4. Particle image velocimetry analysis

[18] An ancillary set of experiments is carried out with 30 g samples of granular material (three tests for each grain size) that are released from behind a gate that is located 12.2 cm above x=0 where this distance is measured along the accelerator (Figure 2). This gate elevation is equal to that used in our earlier experiments [*Cagnoli and Romano*, 2010a and 2010b]. This set of experiments is recorded by a high speed video camera at 1000 fps (resolution: 1024×1024 pixels). The movies have been analysed by particle image velocimetry (PIV) technique [*Pudasaini and Hutter*, 2006; *Raffel et al.*, 2007] to obtain velocity fields of flows that are coming to a halt. For example, Figure 8 presents a sequence of frames illustrating how the speeds of a flow vary during its final deposition.

PIV analyses of the flows before deposition are shown in our earlier papers [e.g., *Cagnoli and Romano*, 2010a].

[19] PIV technique with one video camera allows the measurement of the longitudinal and transversal velocity components of the particles on the surface of the flows. PIV measurements are performed here by subdividing the images into a regular grid of interrogation windows (12×12 pixels in size) and by computing cross-correlation between image pairs separated by 1/1000 s. Our algorithm uses advanced image processing techniques such as window-offset, sub-pixel accuracy and image deformation [*Di Florio et al.*, 2002]. Window overlapping is here equal to 50% and the sampling rate is 1 kHz.

[20] We measure also the longitudinal speed of different portions of each travelling flow when these portions are within an area in a fixed location in the centre of the chute at 10 cm downslope from x=0 (Figure 9). These speeds are those of portions gradually in a more rear position along the flow length as time elapses. These measurements are meant to compare the final speed of the different portions of the different flows before the final deposition. The measuring area (and the flow portion) is 1.5×1.5 cm in size so that it is narrow enough to exclude the more agitated fragments nearer to the containing lateral surfaces. The location, that is the same in all tests, has been selected because it is ~1 cm behind the rear ends of the most proximal deposits (those with coarser grain size) so that all portions of all flows transit through this spot not long before their final deposition. Speeds of all flows must be compared in the same place because their value depends also on the slope angle which is different in different positions on a curved chute. The flows of the ancillary set of experiments travel less than those of the main set (shown in Figure 7) because released from a lower initial elevation.

[21] Figure 9 illustrates sets of measurements of the longitudinal speeds (one example of set for each grain size range) showing that, considering gradually more rear flow portions, their speed (measured in the same spot on the chute) decreases. This refers to the denser part of the flows (black dots in Figure 9) which is shorter in time than the entire time history because the initial and

final sections of these sets of measurements are the speeds of sparser and highly agitated fragments located, respectively, in front and behind the flows (crosses in Figure 9). The positions of the frontal and rear ends of the denser part of the flows are intrinsically fuzzy because of the presence of these sparser fragments whose number increases and agitation decreases toward the flow. Some longitudinal speeds of the sparse fragments (crosses in Figure 9) are smaller than those of the denser part of the flows because these sparse fragments belong to the boundary layer where particles interact directly with the containing boundary surfaces. Because the flows travel in a channel, their boundary layer comes out into view along the flow outline (including at the front and rear ends) and it is visible from above (Figure 1). As shown by particle image velocimetry analysis, the longitudinal speed of the particles on the surface of a flow increases and particle agitation decreases toward the flow (Figure 8 and *Cagnoli and Romano* [2010a, 2010b]). The total mass of all sparse fragments is, in any case, negligible when compared to that of the denser part of the flows. Figure 10 shows the values obtained averaging the speeds of all portions of the denser part of each flow (such as those that in Figure 9 are highlighted as black dots). The smaller the mean grain size, the larger is the speed (Figure 10).

5. Effects of grain size, flow volume and channel width

[22] Particle image velocimetry analysis shows that, during the deposition, the deposit (i.e., the area with particles with zero speed) propagates backward (Figure 8). This means that, on a concave upward slope (Figure 2), such as a volcano flank, the frontal portions of the denser part of a flow are deposited first (because they first reach the less steep parts of the chute), preventing the rear portions (and thus the centre of mass) from travelling further downhill. The fact that the longitudinal speed (measured always in the same position on the chute) decreases when considering gradually more rear portions of the denser part of a flow (Figure 9) confirms that the rear portions of a flow are affected (through internal pressures) by the decelerating or already deposited frontal

portions. This phenomenon, which we expect to occur also on volcano flanks and mountain slopes, is more prominent in larger volume flows because they are longer. This phenomenon is, however, not able to counteract the smaller energy dissipation due to the smaller agitation of fragments per unit of flow mass in the finer grain size flows.

[23] Smaller energy dissipation of finer grain size flows means that they have also larger speeds in the same positions on the chute when compared to coarser grain size flows (Figure 10). When the frontal portions of the denser part of a finer grain size flow stop on a curved slope, the rear portions keep travelling and they do so moving further than in a coarser grain size flow, because finer grain size flows have a larger kinetic energy that causes a larger longitudinal deformation (i.e., shortening) of the deposit. This explains the fact that when comparing deposits with the same volume, those with finer grain size tend to be shorter and wider (Figures 5 and 6). Therefore, also the distance *w* between the channel sidewalls is expected to affect the final position of the centre of mass of the deposit. This is so because the wider the channel, the more room has the deposit to widen laterally and shorten longitudinally so that the more distal is also the centre of mass of the deposit. These observations provide the rationale to formulate some of the scaling parameters discussed in the next section.

6. Dimensional Analysis

[24] We measure the reciprocal of the mobility of a flow by using the apparent coefficient of friction

$$\mu_A = \frac{h}{l}, \tag{2}$$

where h is the vertical drop of the centre of mass of the granular material and l is its horizontal distance of travel. Distances h and l are measured from the position of the centre of mass of the granular samples at rest behind the gate to the position of the centre of mass of the final deposits (Figure 2).

[25] We consider the actual mobility of the centre of mass of a flow (measured as the reciprocal of μ_A) to be a function of several variables including: mean grain size δ [*Cagnoli and Romano*, 2010a], volume V of the deposit, distance w between the channel sidewalls, initial flow speed s, acceleration of gravity g, density ρ_s of the particles, density ρ_f of the intergranular fluid, dynamic viscosity η of the intergranular fluid, angle of internal friction ϕ of the particles, coefficient of restitution e of the rock material and average height i (the roughness) of the ground surface asperities. This corresponds to the following functional relationship:

$$\mu_A = f_1(\delta, V, w, s, g, \rho_s, \rho_f, \eta, \phi, e, i). \tag{3}$$

This is a relationship between twelve variables with three fundamental dimensions (length, time and mass) that, according to the Buckingham Pi theorem, is equivalent to a functional relationship containing nine dimensionless variables. Equation (3) is then replaced by

$$\mu_A = f_2\left(\frac{\delta}{w}, \quad \frac{V^{1/3}}{w}, \quad \frac{\delta g}{s^2}, \quad \frac{\eta}{s \rho_s \delta}, \quad \frac{\delta}{i}, \quad \frac{\rho_f}{\rho_s}, \quad \phi, \quad e\right), \tag{4}$$

which is the relationship between our dependent dimensionless parameter μ_A and the independent dimensionless ones.

[26] The first and second independent dimensionless parameters are, respectively, the scaling of grain size and the scaling of the deposit volume by the channel width because a fragment diameter and a deposit volume can be considered large or small according to the size of the channel width.

The third independent dimensionless parameter is a Froude number which represents a possible scaling of the initial speed [*Cagnoli and Romano*, 2010b]. The fourth independent dimensionless parameter is the ratio of the viscous shear stresses (of the intergranular fluid) to the inertial grain stresses and it corresponds to the reciprocal of the Bagnold number [*Bagnold*, 1954]. The fifth independent parameter represents the importance of the size of the ground asperities relative to the grain size. The sixth parameter is the ratio of fluid density to grain density. Parameters seventh and eight are the angle of internal friction and the coefficient of restitution, respectively, which are already dimensionless variables. Also products of powers of these parameters are legitimate.

[27] The last three independent parameters (ρ_f/ρ_s, ϕ, e) are not responsible for the different mobility of the different flows because their values do not vary in our experiments. The same applies to the fifth independent dimensionless parameter because the asperities of the chute surfaces do not change during our experiments. This is the case because there is no observed larger mobility of the same type of flows in experiments repeated later during the experimental session (when compared with earlier experiments) that can be due to a possible smoothing of the chute surfaces with time. The Bagnold number (that, with a characteristic speed measured in the same spot on the chute for all flows, corresponds, as far as the role played by η is concerned, to the reciprocal of our fourth independent dimensionless parameter) has values in our experiments that are significantly larger than the critical threshold equal to ~450 [*Iverson and Denlinger*, 2001] indicating that the dynamics of our flows is dominated by particle collisions [*Bagnold*, 1954]. Therefore, the viscosity of the intergranular fluid (air) is relatively too small for air to affect our particle dynamics and, thus, flow mobility. The third independent dimensionless parameter (which is the scaling of the initial speed) is not considered here, because all our flows have an initial speed equal to zero.

[28] Other variables whose values do not vary in our experiments are not included in equation (3). For example, form, angularity and surface texture of the particles of our different flows are not significantly different (Figure 3). Furthermore, high pore pressures (if any) should dissipate quickly in a shallow open channel because of the relatively large pore pressure diffusivity that is expected

in dry flows that are dilated because of particle collisions (and, in any case, relatively more so in contact with the boundary surfaces). For example, with relatively not too fine grains, the effects of an initial gas fluidisation dissipate very quickly. In our flows, the Savage number has values larger than the threshold equal to 0.1 confirming a larger importance of grain collision stresses at the base of the flows [*Savage and Hutter*, 1989]. Only the finer grain size (0.5-1 mm) flows with the larger mass (60 g) have a Savage number value smaller than this threshold. The Savage number represents the ratio of grain collision stresses to gravitational grain contact stresses that produce Coulomb's friction [*Iverson and Denlinger*, 2001]. Estimates of the Savage number are, however, difficult because of difficulties in estimating the shear strain rate during flow motion.

[29] We consider the first and second independent dimensionless parameters as those containing the variables whose different values are responsible for the differences in the final positions of the centre of mass of the deposits. Therefore

$$\mu_A = f_3\left(\frac{\delta}{w}, \frac{V^{1/3}}{w}\right). \tag{5}$$

In particular, the experiments (Figure 11) demonstrate that

$$\mu_A = \mathrm{a}\beta + \mathrm{b}\,, \tag{6}$$

where

$$\beta = \frac{\delta}{w}\frac{V^{1/3}}{w} = \frac{\delta\, V^{1/3}}{w^2}\,. \tag{7}$$

Here, coefficient a is 0.0217 and coefficient b is 0.8184. The correlation coefficient r (which measures the linear relationship between two variables [*Davis*, 1986]) has a value equal to 0.98. We

adopt a value for w equal to the smallest distance (6 mm) between the inclined sidewalls (inset in Figure 2), because the width at the base of a channel that is trapezoidal in cross section concerns the flows more than that at the top that is larger than the flow width.

[30] When multiplied by δ/δ, parameter β can be written as $V^{1/3}/\delta$ (=Γ) multiplied by δ^2/w^2 (=$1/\gamma$). Γ is proportional to the number of particles in the flow (because it corresponds to V/δ^3) whereas γ is proportional to the number of particles whose sum of cross-sectional areas covers completely a portion of chute surface equal to w^2 (because the central cross-sectional area of a particle is proportional to δ^2). Therefore,

$$\beta = \frac{\Gamma}{\gamma}. \tag{8}$$

Parameter β is inversely proportional to γ, because the larger the number of particles per unit of flow mass, the smaller is the penetration within the flow of particle agitation due to the interaction with the rough sidewalls (Figure 1) and, consequently, the smaller is the energy dissipated per unit of travel distance [*Cagnoli and Romano*, 2010a]. Parameter β is proportional to Γ (which is proportional to the flow length) because, the longer the flow, the more prominent is the effect of the frontal part of a flow that reaches the less steep portion of a curved chute and stops before the rear part preventing the rear part (and the centre of mass) from travelling further downhill (section 5). Equations (5) and (6) have a different number of dimensionless parameters. However, we obtain an equation (5) with only two parameters (μ_A and β) if Γ / γ replaces V and w in equation (3).

[31] The fact that all the experimental points lie along a single curve (Figure 11) confirms that only the variables considered in equation (6) have an effect on the position of the centre of mass of the deposits of the different flows. Importantly, the experimental points lie along a single curve also regardless of the value of the Savage number that can be, indifferently, larger or smaller than the

threshold equal to 0.1. The fact that the data of the same type of flows are well grouped suggests an excellent repeatability of the experiments.

7. Discussion

[32] In the plot of μ_A versus β, the intercept of the fitted straight line with the vertical axis is in a position different from the origin because the energy dissipation of any flow is always larger than zero and, for this reason, the apparent coefficient of friction cannot be equal to zero (Figure 11). The apparent coefficient of friction μ_A has relatively large values in the range 0.82-0.87 (Figure 11). Similar values were obtained also for flows with the same characteristics that were released from behind a gate located at a lower elevation [*Cagnoli and Romano*, 2010a]. Figure 11 shows that basal and lateral frictions do not depend only on the roughness i of the slope surfaces but also on the characteristics of the flows because in our experiment we do not change the characteristics of the slope. It is for this reason that the friction parameter μ_A is the dependent variable on the left hand side of equations (3) and (6).

[33] The frontal end of larger volume deposits (all the other features the same) is in a more distal position than the frontal end of smaller volume deposits (Figure 7). Therefore, geologists that find the consequent more distal outcrops in the field end up concluding that larger volume flows are more mobile. For example, *Scheidegger* [1973] reports values of the apparent coefficient of friction that decrease from ~0.9 to less than 0.1 as volume increases, and other authors [e.g., *Sparks*, 1976; *Nairn and Self*, 1978; *Hayashi and Self*, 1992] obtain particularly small values. But these small values have not been obtained considering the position of the centre of mass [*Hayashi and Self*, 1992]. Similar trends with relatively smaller apparent friction values can be obtained also in our experiments as shown by Figure 12, where the ratio h/l is computed considering the vertical and horizontal distances from the rear end of the granular samples behind the gate to the frontal end of

the deposits (this type of h/l ratio is called here R). R, as shown by his figure, is the parameter that *Scheidegger* [1973] refers to.

[34] The use of the position of the frontal end of a deposit generates relatively small values of the apparent coefficient of friction (Figure 12) that are not useful for an energy dissipation analysis. This is so because it is the location of the entire deposit that needs to be considered with, for example, the positions of the maximum width and maximum depth. Larger volume deposits tend to have also more proximal rear ends (Figure 7). Larger volumes have, thus, a larger longitudinal spreading [*Davies*, 1982; *Manzella and Labiouse*, 2009]. In an energy dissipation analysis, it is the definition of flow mobility we adopt here, based on the distance travelled by the centre of mass, that is useful, because the centre of mass of a system of bodies is the point that moves as though all mass were concentrated there and all external forces were applied there.

[35] Our experiments show that the effect of volume on the mobility of the flows is multifaceted. On one hand, we expect that larger volume flows, all the other features equal, dissipate relatively less energy per unit of flow mass because they have less agitated fragments per unit of flow mass (Figure 1) [*Cagnoli and Romano*, 2010a, 2010b]. On the other hand, larger volume flows (for the reason that they are longer) prevent more their centre of mass from travelling further downhill when their frontal part reaches the less steep portion of a curved chute and stops before the rear part preventing the rear part from moving further downhill. We adopt parameter μ_A to assess which of these two phenomena prevail. This parameter is useful because it is the reciprocal of the horizontal distance of travel normalised by the initial elevation. For obvious geometric reasons, the centres of mass of larger volume samples behind the gate have higher initial elevations than those of smaller volume. Therefore, the fact that the position of the centres of mass of larger volume deposits tends to be more distal than that of smaller volume deposits (see for example the finer grain size data in Figure 13) can be explained by the larger initial potential energy. Thus, a normalisation by the initial elevation is necessary.

[36] All this considered, the apparent coefficient of friction of larger volume flows is larger than that of smaller volume flows with the same grain size (Figure 11). Therefore, the phenomenon which consists in the frontal portions of the flows that stop before the rear portions is able to counteract the relatively smaller energy dissipation due to less agitated fragments per unit of flow mass that is expected in larger volume flows. It is, however, unable to counteract the increase in mobility due to a decrease of grain size (Figure 11).

[37] However, larger volume flows (all the other features the same) have also a more distal position of the frontal end of their deposits (Figure 7). This is due to the fact that the larger the volume of the deposits, the larger is the longitudinal spreading both upslope and downslope relative to their centres of mass (this is easy to see if in Figure 7 we imagine the centres of mass coincident). This can be understood observing that when comparing deposits with different volumes, the difference between their length (a few centimetres here) is larger in magnitude than the difference between their maximum thickness (only a few millimetres here). Therefore, the mass difference modifies mainly the length and larger volume deposits are much longer than they are thicker when compared to smaller volume ones. The larger longitudinal spreading of larger volume deposits is an important feature to consider (together with the actual mobility of the centre of mass) when hazards are assessed in mountain regions.

[38] We expect the rear portion of a flow (on the steeper part of a curved slope) to push downhill its frontal portion and the frontal portion (on the less steep part of the curved slope) to hinder the motion of the rear portion. The position of the centre of mass of the final deposit is the result of these behaviours, where the frontal portion holds back the rear portion in relatively more proximal positions when the flow is longer (i.e., its volume larger). In longer flows, the rear end of the deposits (and their centre of mass, when normalisation by the initial elevation is considered) will be in relatively more proximal positions (Figure 11) because the rear and the frontal ends are more distant than in shorter flows.

[39] Our experiments confirm also another important behaviour [*Cagnoli and Romano*, 2010a] that is important to consider in hazard assessments: the centres of mass of finer grain size flows are more mobile than those of coarser grain size flows (Figure 11). The fact that flow speeds of finer grain size flows are larger (because they dissipate less energy per unit of travel distance) than those of coarser grain size flows (all the other features equal), means also that, in the same place, they have larger impact velocities if they find obstructions on their way (Figure 10).

[40] Departures from the assumption of densities uniform in space in the granular samples behind the gate and in the final deposits (each one with its own value of density) can affect the estimates of the position of the centres of mass. However, visual inspection of the large upper surfaces of these relatively thin deposits and the fact that the granular material behind the gate has always been compacted uniformly (always following the same procedure) suggest that this assumption is good. The presence of possible larger spaces (due to arch effects) that are randomly distributed within the granular masses are not expected to affect the position of the average of the centres of mass of the deposits with the same features. If there were differences in the energy dissipation of the initial deformation of the granular masses as function of their features, they would be intrinsic to (and would give a contribution to explain), for example, the observed volume effect. However, we obtained a linear trend of μ_A versus β also with granular flow masses as small as 5 and 15 g. This suggests that the larger granular masses (60 g for example) are not affected by a disproportionate friction in contact with gate and sidewalls within the accelerator. The same trend shown in Figure 11 has been obtained also rotating forward the gate instead of sliding it upward and it has been obtained also with the gate in different positions along the accelerator.

[41] The idea that flows with more agitated particles per unit of flow mass dissipate more energy and travel less does not contradict other authors' suggestion that dilated granular flows are more mobile [e.g., *Davies*, 1982]. This is so if they mean that dilated flows are more mobile than non-dilated flows that are slipping (i.e., travelling flows whose basal non-colliding particles are in continuous contact with the ground surface). Slipping flows on a rough ground surface must have a

small speed to be non-dilated. As soon as the speed of these flows increases, they become dilated because particle collisions with the ground surface asperities generate slope-normal components of particle velocities. These dilated flows are then more mobile because of their larger speed. For dilated flows with the same speed, however, the larger the particle agitation per unit of flow mass (all the other features the same), the smaller is the travel distance [*Cagnoli and Romano,* 2010a].

8. Conclusions

[42] The potential mobility of a flow (i.e., its intrinsic ability to dissipate more energy or less energy in a single spot on the chute) depends on its features such as grain size and flow volume. In particular, the finer the grain size or the larger the flow volume (all the other features the same), the smaller is the energy dissipated per unit of flow mass [*Cagnoli and Romano,* 2010a and 2010b]. This is due to the fact that in finer grain size flows or in larger volume flows (all the other features equal), there is a larger number of particles, so that their agitation due to the interaction with the rough containing boundary surfaces penetrates relatively less inside the flows (Figure 1). Flows whose particles are less agitated per unit of flow mass dissipate less energy per unit of travel distance. However, the final position of the centre of mass of a deposit (i.e., the actual flow mobility) depends also on other phenomena. For example, on curved slopes (such as volcano flanks), the frontal portion of a flow reaches the less steep part of the slope and stops before the rear portion preventing the rear portion, and the centre of mass, from travelling further downhill.

[43] For the purpose of analyzing quantitatively the effect of grain size and flow volume on the actual mobility of the centre of mass of granular flows of angular rock fragments, we carried out a dimensional analysis of experimental data. Our experiments show that a straight line is the functional relationship between the dimensionless apparent coefficient of friction and a scaling parameter whose numerator is equal to the mean grain size multiplied by the cube root of the deposit volume and whose denominator is the square of the channel width (equation (6)). This

relationship shows that the apparent coefficient of friction measured considering the distance travelled by the centre of mass of larger volume flows is larger than that of smaller volume flows with the same grain size. This relationship confirms also that the finer the grain size of the flows, the larger is the mobility of their centre of mass.

[44] Our experiments show also that larger volume flows (all the other features the same) have a longitudinal spreading that is larger than that of smaller volume flows. Therefore, even if the apparent coefficient of friction of larger volume flows (all the other features the same) is larger, the frontal ends of their deposits are located in a more distal position than those of smaller volume flows. This is also an important phenomenon (together with the actual mobility of the centre of mass of the flows) that needs to be considered when natural hazards are assessed in mountain regions.

[45] **Acknowledgments.** We are grateful to Enzo Boschi and Antonio Piersanti for their support. We thank Domenico Pietrogiacomi for his assistance in the laboratory. We thank also the reviewers for their useful comments.

References

Bagnold, R.A. (1954), Experiments on a gravity-free dispersion of large solid spheres in a Newtonian fluid under shear, *Proc. R. Soc. London*, *225*, 49-63.

Banton, J., P. Villard, D. Jongmans, and C. Scavia (2009), Two-dimensional discrete element models of debris avalanches: Parameterization and the reproducibility of experimental results, *J. Geophys. Res.*, *114*, F04013, doi:10.1029/2008JF001161.

Becker, G.F. (1905), A feature of Mayon Volcano, *Proc. Wash. Acad. Sci.*, *7*, 277-282.

Cagnoli, B., and M. Manga (2003), Pumice-pumice collisions and the effect of the impact angle, *Geophys. Res. Lett.*, *30*, 1636. doi:10.1029/2003GL017421.

Cagnoli, B., and M. Manga (2004), Granular mass flows and Coulomb's friction in shear cell experiments: Implications for geophysical flows, *J. Geophys. Res.*, *109*, F04005. doi:10:1029/2004JF000177.

Cagnoli, B., and M. Manga (2005), Vertical segregation in granular mass flows: A shear cell study, *Geophys. Res. Lett.*, *32* (L10402). doi:10:1029/2005GL023165.

Cagnoli, B., and F. Quareni (2009), Oscillation-induced mobility of flows of rock fragments with quasi-rigid plugs in rectangular channels with frictional walls: A hypothesis, *Eng. Geol.*, *103*, 23-32.

Cagnoli, B., and G.P. Romano (2010a), Effect of grain size on mobility of dry granular flows of angular rock fragments: An experimental determination, *J. Volcanol. Geotherm. Res.*, *193*, 18-24.

Cagnoli, B., and G.P. Romano (2010b), Pressures at the base of dry flows of angular rock fragments as a function of grain size and flow volume: Experimental results, *J. Volcanol. Geotherm. Res.*, *196*, 236-244.

Cagnoli, B., P.L. Rossi, C.A. Tranne and L. Vigliotti (1994), Facies and paleomagnetic characteristics of a pyroclastic flow deposit in Ustica Island (South Tyrrhenian Sea), *Acta Vulcanol.*, *5*, 1-9.

Cas, R.A.F., and J.V. Wright (1988), *Volcanic successions*, Unwin Hyman, London.

Davies, T.R.H. (1982), Spreading of rock avalanche debris by mechanical fluidization, *Rock Mech.*, *15*, 9-24.

Davis, J.C. (1986), *Statistics and data analysis in geology*, John Wiley and Sons, New York.

Dellino, P., B. Zimanowski, R. Büttner, L. La Volpe, D. Mele, and R. Sulpizio (2007), Large-scale experiments on the mechanics of pyroclastic flows: Design, engineering and first results, *J. Geophys. Res.*, *112*, B04202, doi:10.1029/2006JB004313.

Di Florio, D., F. Di Felice, and G.P. Romano (2002), Windowing, re-shaping and re-orientation interrogation windows in particle image velocimetry for the investigation of shear flows, *Meas. Sci. Technol.*, *13* (7), 953-962.

Félix, G., and N. Thomas (2004), Relation between dry granular flow regimes and morphology of deposits: formation of levées in pyroclastic deposits, *Earth Planet. Sci. Lett.*, *221*, 197-213.

Goldsmith, W. (2001), *Impact: the theory and physical behaviour of colliding solids*, Dover Publications, New York.

Hayashi, J., and S. Self (1992), A comparison of pyroclastic flow and debris avalanche mobility, *J. Geophys. Res.*, *97*(B6), 9063-9071.

Holtz, R.D., and W.D. Kovacs (1981), *An Introduction to Geotechnical Engineering*, Prentice-Hall, New Jersey.

Hutter, K., and T. Koch (1991), Motion of a granular avalanche in an exponentially curved chute: experiments and theoretical predictions, *Phil. Trans. R. Soc. Lond.*, *334*, 93-138.

Jop, P., Y. Forterre, and O. Pouliquen (2006), A constitutive law for dense granular flows, *Nature*, *441*, 727-730.

Iverson, R.M., and R.P. Denlinger (2001), Flow of variably fluidized granular masses across three-dimensional terrain, 1. Coulomb mixture theory, *J. Geophys. Res.*, *106* (B1), 537-552.

Lube, G., S.J. Cronin, T. Platz, A. Freundt, J.N. Procter, C. Henderson, and M.F. Sheridan (2007), Flow and deposition of pyroclastic granular flows: A type example from the 1975 Ngauruhoe eruption, New Zealand, *J. Volcanol. Geotherm. Res.*, *161*, 165-186.

Lube, G., H.E. Huppert, R.S.J. Sparks, and A. Freundt (2011), Granular column collapses down rough, inclined channels, *J. Fluid Mech.*, *675*, 347-368.

Lucas, A., and A. Mangeney (2007), Mobility and topographic effects for large Valles Marineris landslides on Mars, *Geophys. Res. Lett.*, 34, L10201, doi:10.1029/2007GL029835.

Manzella, I., and V. Labiouse (2009), Flow experiments with gravel and blocks at small scale to investigate parameters and mechanisms involved in rock avalanches, *Eng. Geol.*, 109, 146-158.

McArdell, B.W., P. Bartelt, and J. Kowalsky (2007), Field observations of basal forces and fluid pore pressure in a debris flow, *Geophys. Res. Lett.*, *34*, L07406, doi:10.1029/2006GL029183.

Nairn, I.A., and S. Self (1978), Explosive eruptions and pyroclastic avalanches from Ngauruhoe in February 1975, *J. Volcanol. Geotherm. Res.*, *3*, 39-60.

Pudasaini, S.P., and K. Hutter (2006), *Avalanche dynamics*, Springer, Berlin.

Raffel, M., C.E. Willert, S.T. Wereley, and J. Kompenhans (2007), *Particle Image Velocimetry*, Springer, Berlin.

Rowley, P.D., M.A. Kuntz, and N.S. MacLeod (1981), Pyroclastic-flow deposits, in *The 1980 eruptions of Mount St. Helens, Washington*, edited by P.W. Lipman and D.R. Mullineaux, U.S. Geol. Surv. Prof. Pap., 1250, pp. 489-512.

Saucedo, R., J.L. Macías, and M. Bursik (2004), Pyroclastic flow deposits of the 1991 eruption of Volcán de Colima, Mexico, *Bull. Volcanol.*, *66*, 291-306.

Savage, S.B., and K. Hutter (1989), The motion of a finite mass of granular material down a rough incline, *J. Fluid Mech.*, *199*, 177-215.

Scheidegger, A.E. (1973), On the prediction of the reach and velocity of catastrophic landslides, *Rock Mech.*, *5*, 231-236.

Sparks, R.S.J. (1976), Grain size variations in ignimbrites and implications for the transport of pyroclastic flows, *Sedimentology*, *23*, 147-188.

Takahashi, T., and H. Tsujimoto (2000), A mechanical model for Merapi-type pyroclastic flow, *J. Volcanol. Geotherm. Res.*, *98*, 91-115.

Voight, B., and J. Sousa (1994), Lessons from Ontake-san: A comparative analysis of debris avalanche dynamics, *Eng. Geol.*, *38*, 261-297.

Zenz, F.A., and D.F. Othmer (1960), *Fluidization and Fluid-Particle Systems*, Reinhold, New York.

FIGURE CAPTIONS

Figure 1. These illustrations portray particle agitation per unit of flow mass that increases as grain size (δ) increases or as flow volume (V) decreases (all the other features the same). In this figure, the more agitated particles are represented by more separated polygons. Agitation is larger nearer to the rough containing boundary surfaces. These sketches are based on a study of high speed video camera images.

Figure 2. Longitudinal cross section of experimental apparatus. Quantity h is the vertical drop of the centre of mass and quantity l is its horizontal distance of travel. CM stands for centre of mass. Inset shows transversal cross section of channel that is trapezoidal in shape.

Figure 3. Angular rock fragments used in the experiments. The grain size of the mixtures increases from left to right (0.5-1, 1-2 and 2-3 mm respectively).

Figure 4. (a) Mature shape of travelling flow, (b) its deposit and (c) the distal distribution of individual fragments. The grain size of this flow is in the range 0.5-1 mm. The arrows show the flow direction. Numbers in the tape measure are the centimetres on the chute from x=0.

Figure 5. Maximum width of deposits. Values in millimetres are the grain size ranges and the values in grams the initial flow masses. Finer grain size deposits with the same volume are wider.

Figure 6. Longitudinal spreading of deposits. Values in millimetres are the grain size ranges and the values in grams the initial flow masses. Finer grain size deposits with the same volume are shorter.

Figure 7. This figure shows the position along the chute of the longitudinal spreading (represented by the length of the vertical segments) of the deposits. Distances are measured along the curved slope. The position of the centre of mass is represented by a black circle. Values in millimetres are the grain size ranges and the values in grams are the initial flow masses.

Figure 8. Velocity fields obtained by particle image velocimetry (PIV) analysis of upper surface of a flow that is coming to a halt imaged from above by a high-speed video camera. The grain size range of the flow is in millimetres and the value in grams is the initial flow mass. The values in centimetres, on the left side of the figure, are the distances from x=0 along the chute. Values in ms are the distances in time from the first frame on the left. The longitudinal components of particle speeds are colour coded. The maximum speeds are relatively small in value because the particles are imaged just before their final deposition. The colour yellow outlines the moving part of the flow whereas the colour orange represents the background with no particles and the particles with zero speed (i.e., the deposit). The sequence of frames shows that the deposit propagates backwards.

Figure 9. Each data point is the longitudinal speed of a portion of a travelling flow measured by particle image velocimetry analysis. The speed is measured when this portion (1.5×1.5 cm in size) is located at 10 cm from x=0 in the centre of the chute. Thus, these speeds are those of portions gradually in a more rear position along the flow length as time elapses. Black dots are speeds of the portions of the denser part of the flows. The crosses represent speeds of sparser and highly agitated particles in front and behind the flows. Values in millimetres are the grain size ranges and the values in grams the initial flow mass. The speeds of the rear portions of the denser part of all flows are smaller than those of the frontal portions. Finer grain size flows are faster than coarser ones.

Figure 10. Averages of the longitudinal speeds of the different portions of the denser part of each flow (such as those represented by black dots in Figure 9) versus the mean grain size of the granular mixtures. In this figure, the flows have initial masses equal to 30 g. Finer grain size flows are faster than coarser ones.

Figure 11. Parameter μ_A is the apparent coefficient of friction. Parameter β is the product of the mean grain size by the cube root of the deposit volume divided by the square of the channel width. Values in millimetres are the grain size ranges and the values in grams the initial flow masses. The least squares fit to the data is a straight line.

Figure 12. R is an h/l ratio computed considering the horizontal and vertical distances from the rear end of the granular samples at rest behind the gate to the frontal end of the final deposits. Values in millimetres are the grain size ranges and values in grams the initial flow masses. The fitted curve is a straight line.

Figure 13. Non-normalised position of the centre of mass of the deposits in the Cartesian reference frame shown in Figure 2. Values in millimetres are the grain size ranges and the values in grams the initial flow masses. The dotted line represents the base of the channel on the slope.

Table 1. Mean length of deposits with error of the mean versus grain size and flow mass.

	2-3 mm	1-2 mm	0.5-1 mm
30 g	22.8±0.6 cm	22.9±0.2 cm	20.9±0.2 cm
60 g	27.3±0.3 cm	25.6±0.3 cm	24.1±0.4 cm

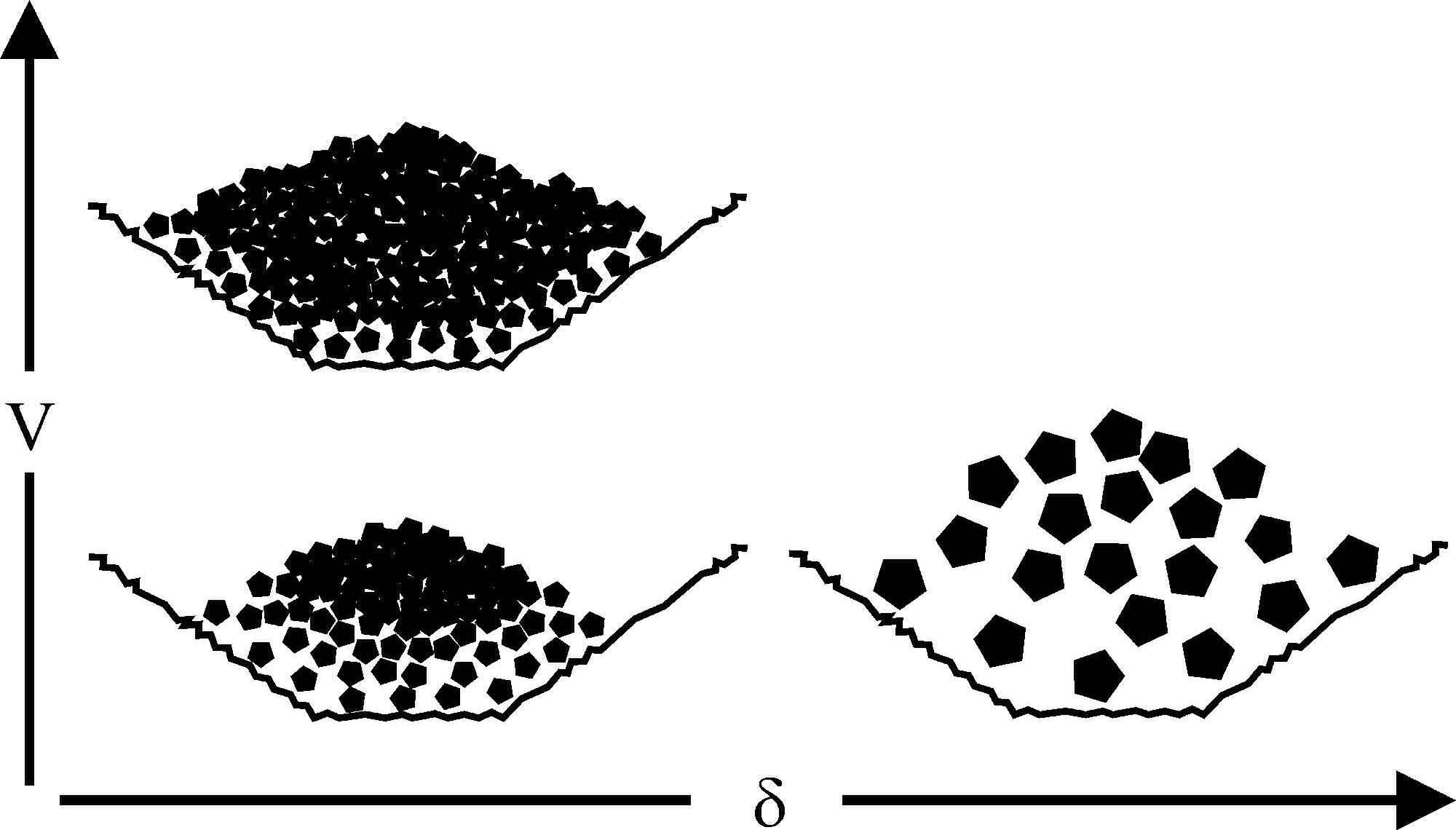
V
δ

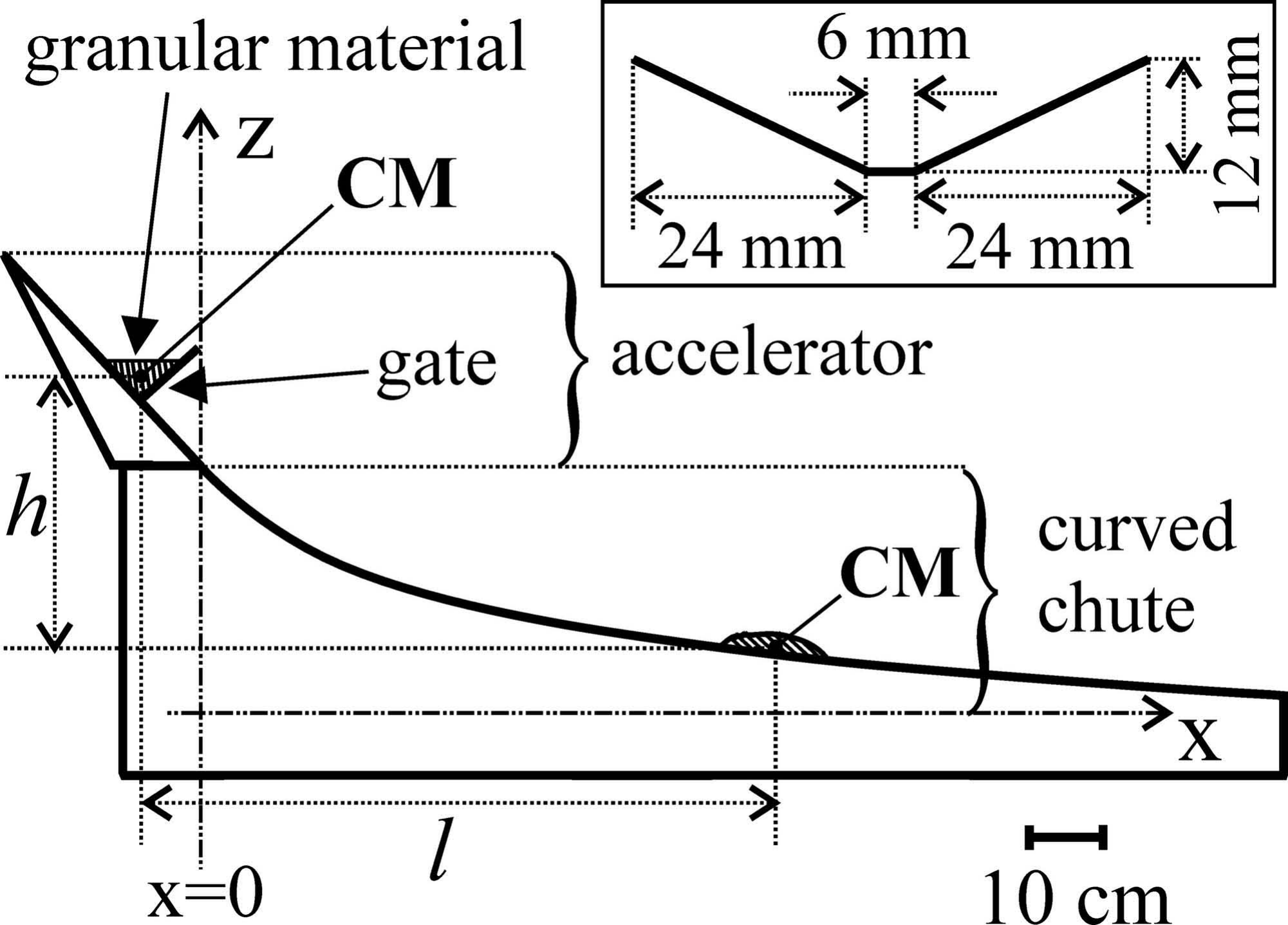
granular material
z
CM
gate
accelerator
h
CM
curved
chute
x
x=0
l
10 cm
6 mm
12 mm
24 mm
24 mm


mm

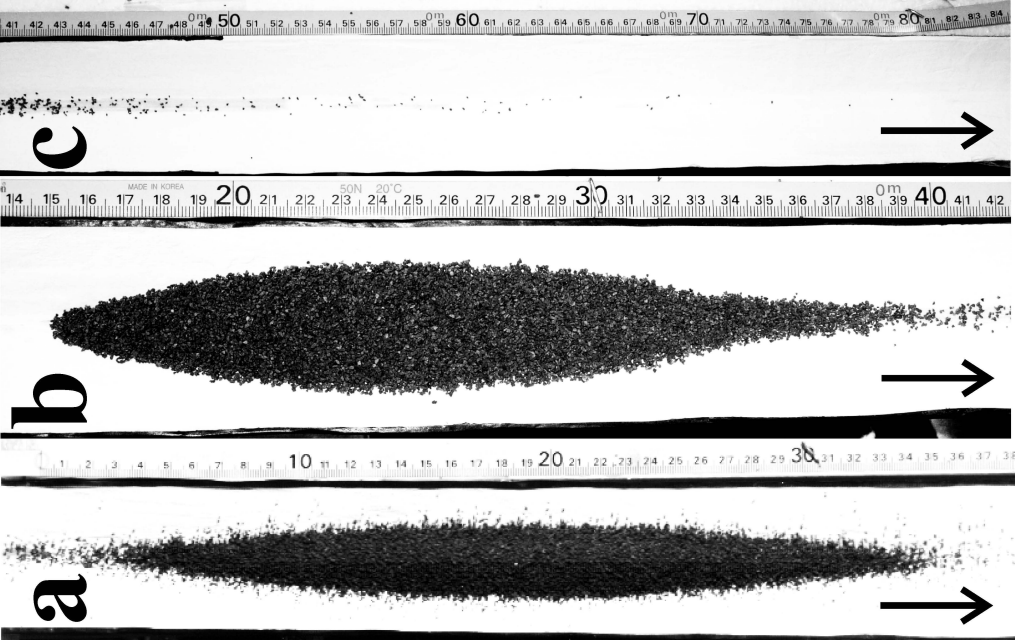
c
b
a
MADE IN KOREA
50N 20°C

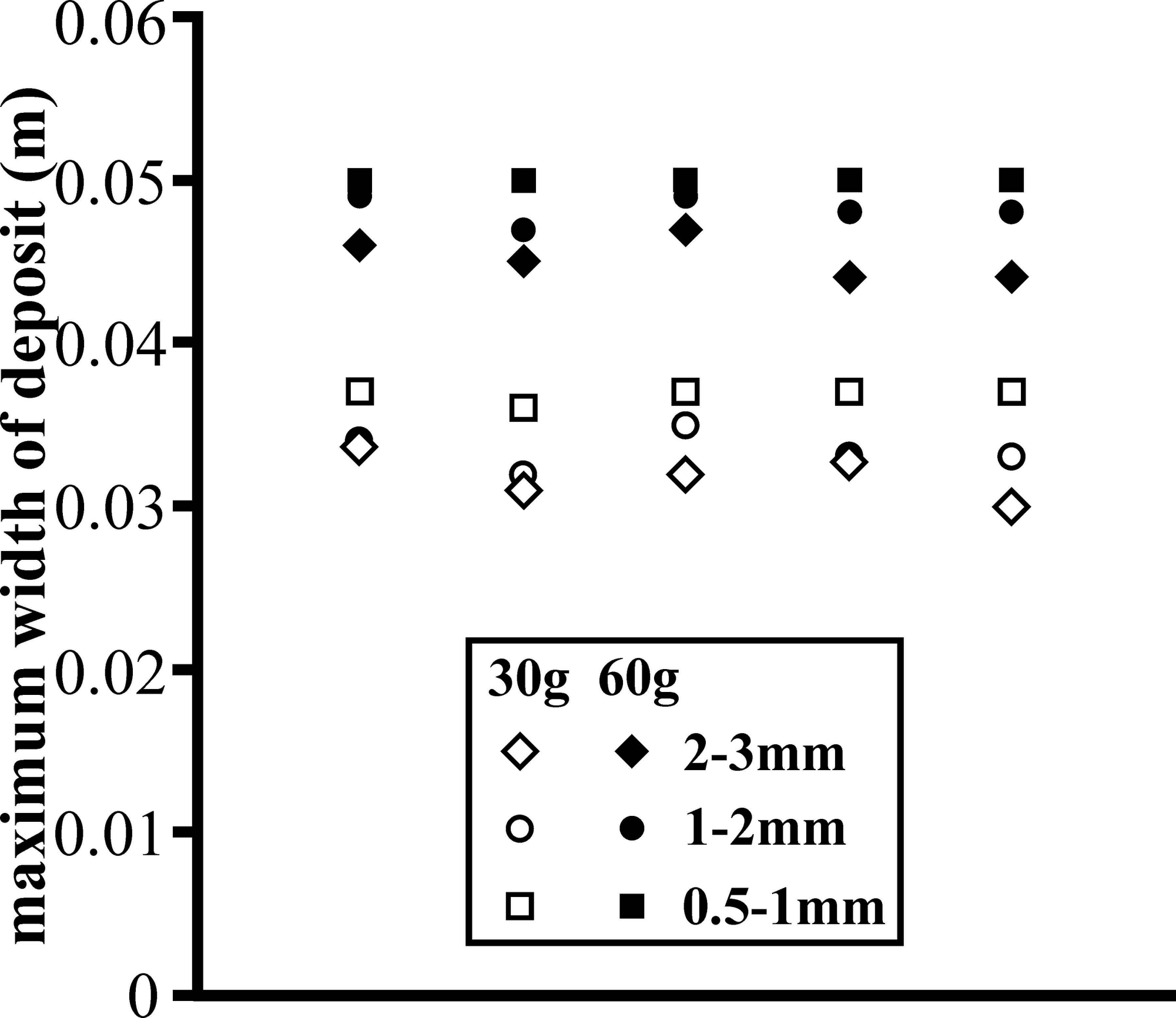
maximum width of deposit (m)
0.06
0.05
0.04
0.03
0.02
0.01
0
30g 60g
2-3mm
1-2mm
0.5-1mm

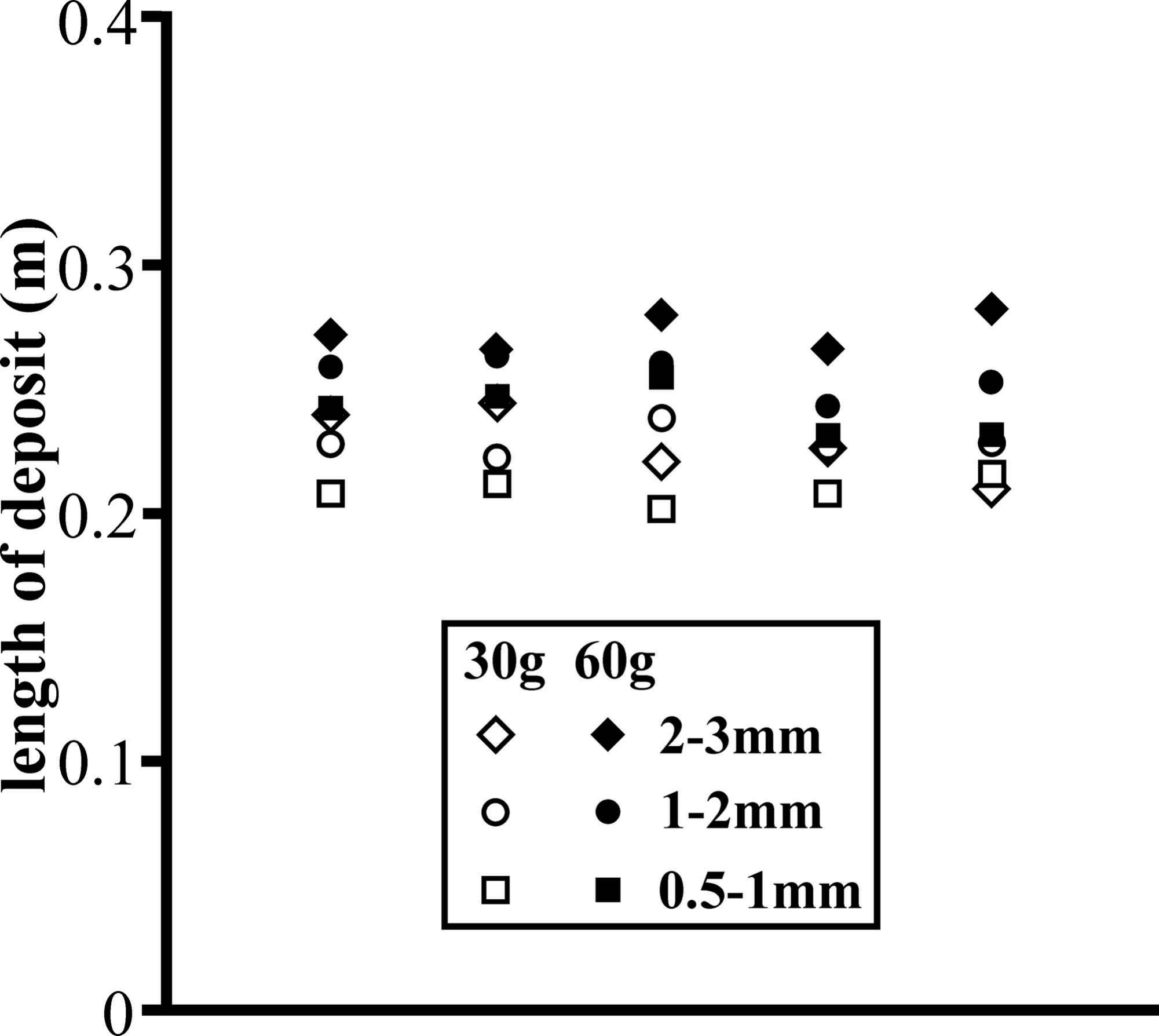
length of deposit (m)
0.4
0.3
0.2
0.1
0
30g 60g
2-3mm
1-2mm
0.5-1mm

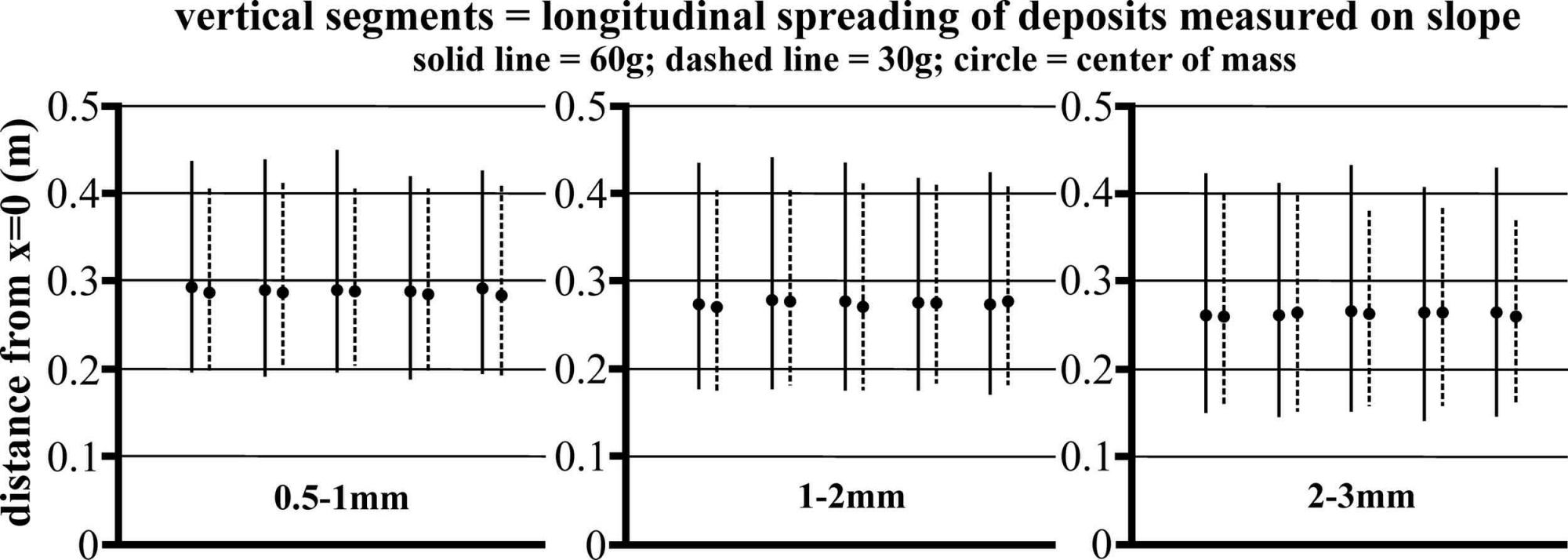
vertical segments = longitudinal spreading of deposits measured on slope
solid line = 60g; dashed line = 30g; circle = center of mass
distance from x=0 (m)
0.5
0.4
0.3
0.2
0.1
0
0.5-1mm
1-2mm
2-3mm

10cm
20cm
30cm
40cm
0.5-1mm; 30g
Flow direction
0m/s
0.8m/s
100 ms
Deposit propagation
150 ms
Deposit propagation
200 ms
Deposit propagation
250 ms
Deposit propagation
2cm

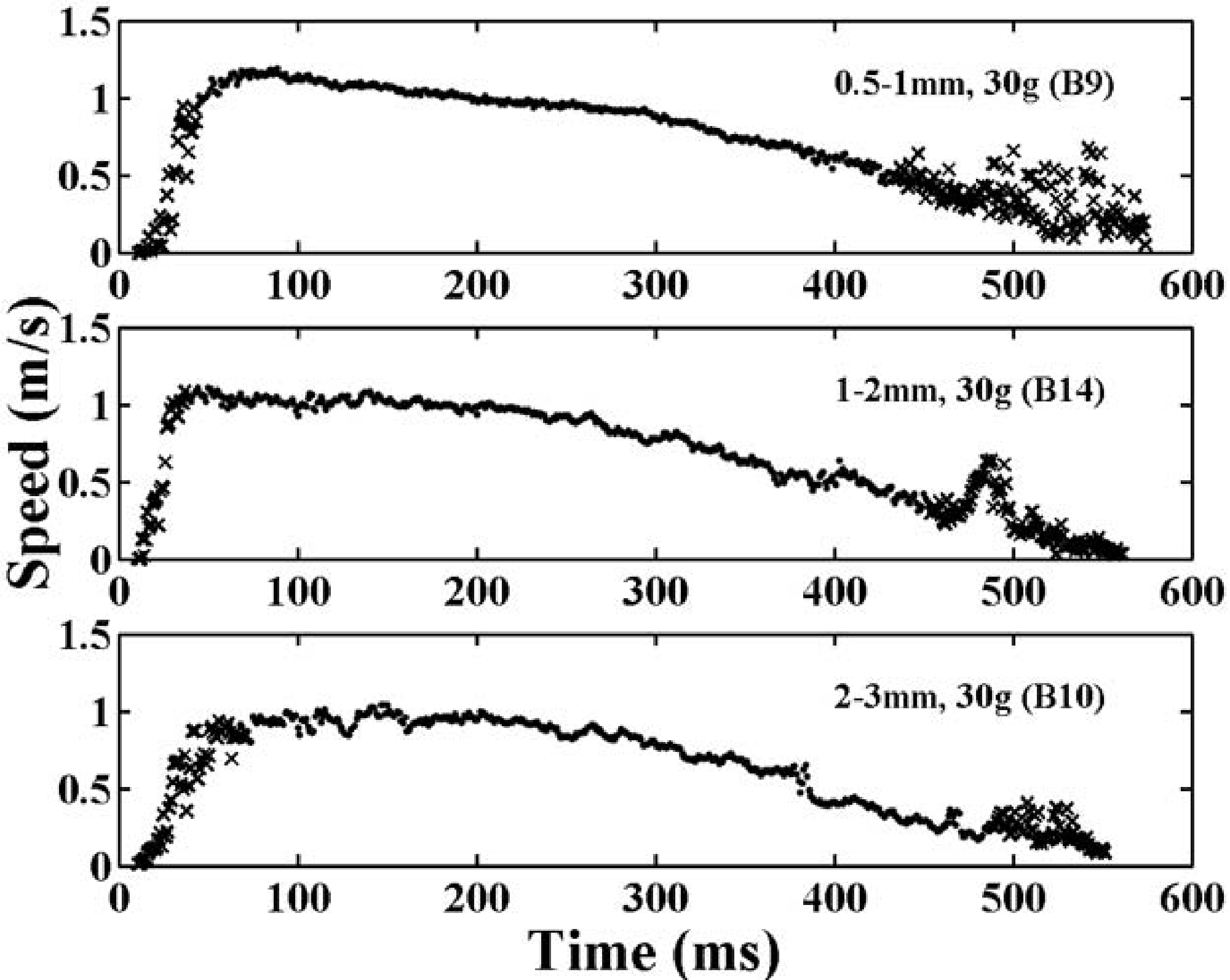
0.5-1mm, 30g (B9)
1-2mm, 30g (B14)
2-3mm, 30g (B10)
Speed (m/s)
Time (ms)
0
0.5
1
1.5
0
100
200
300
400
500
600

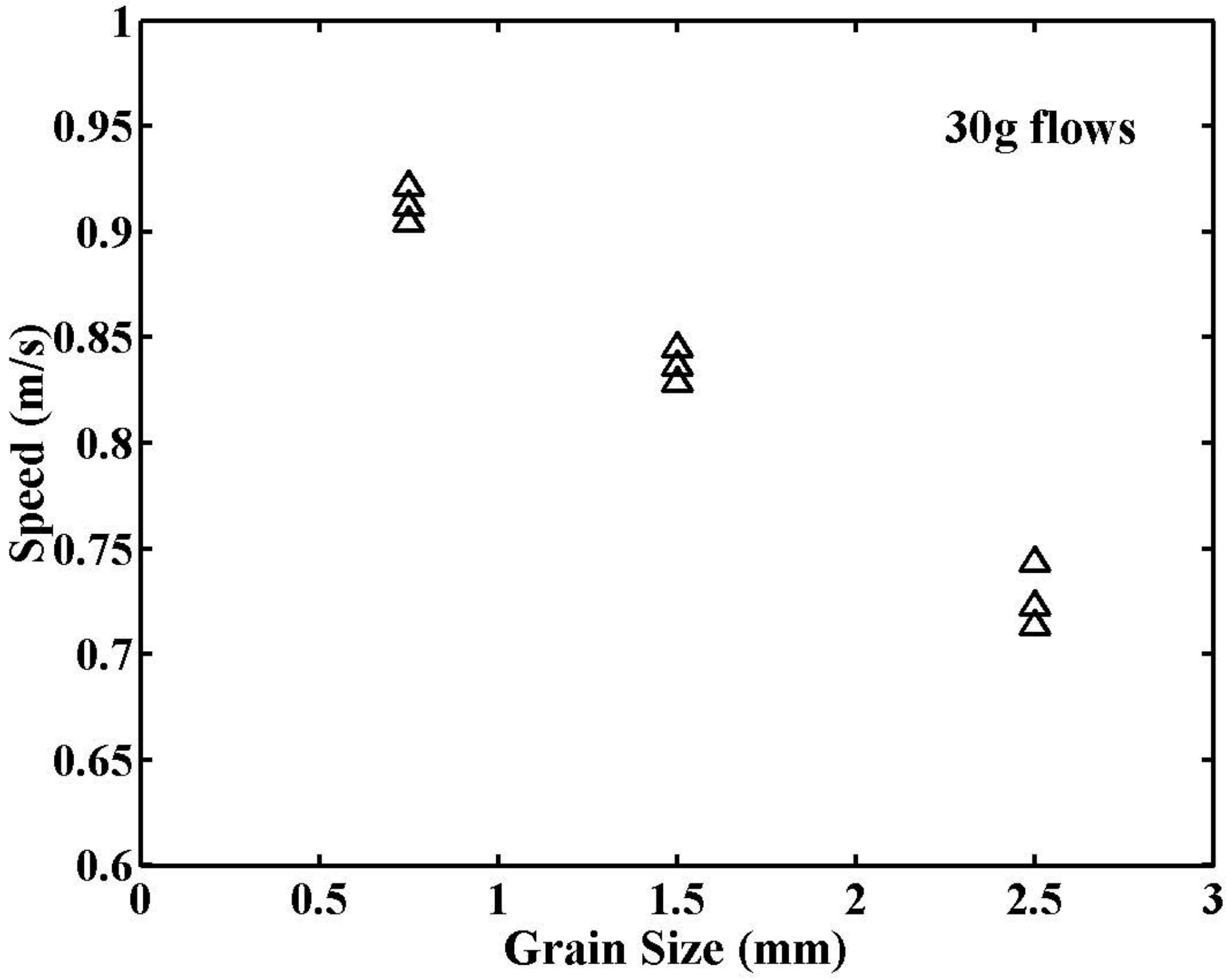
30g flows
Speed (m/s)
Grain Size (mm)
1
0.95
0.9
0.85
0.8
0.75
0.7
0.65
0.6
0
0.5
1
1.5
2
2.5
3

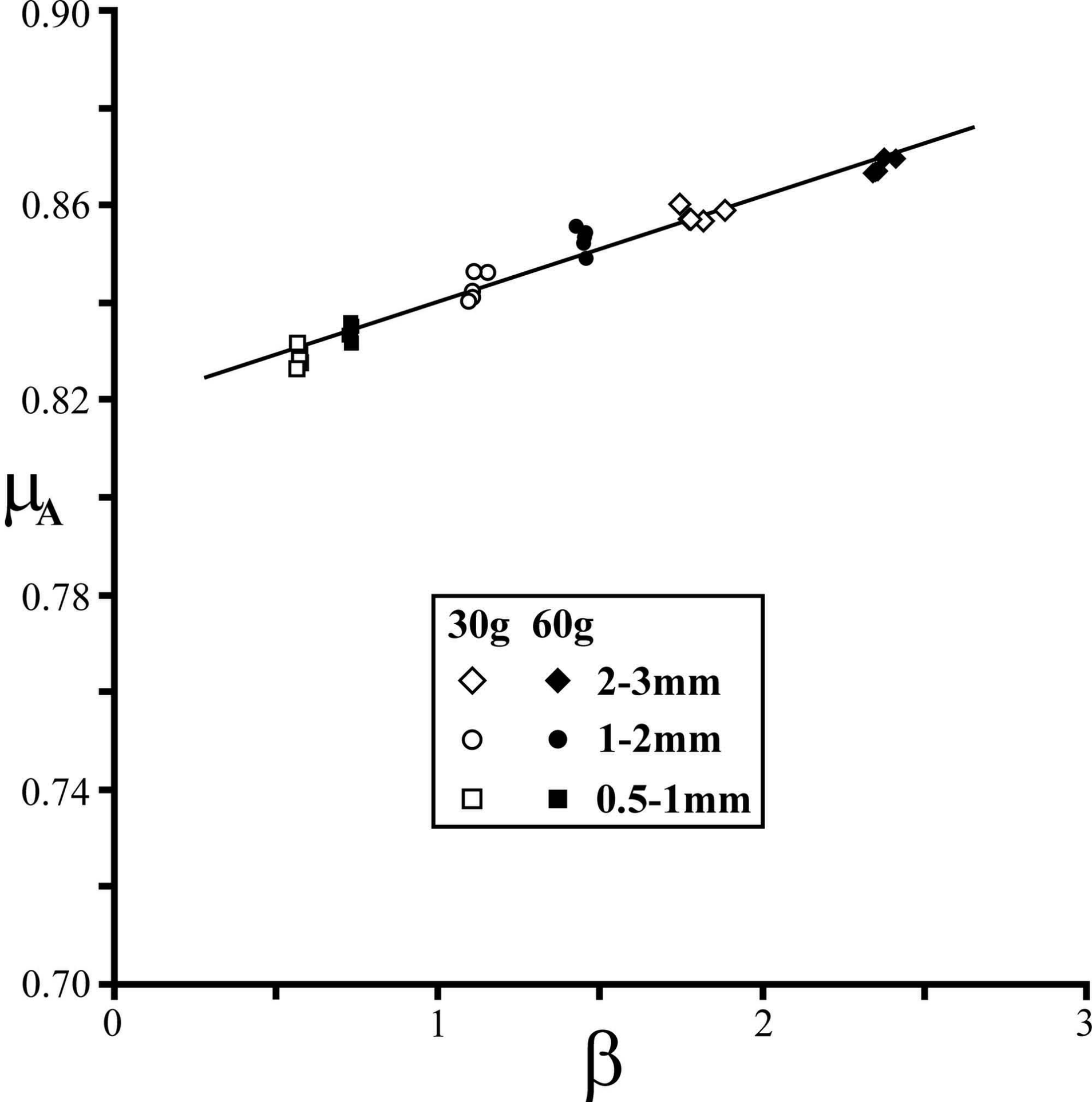
0.90
0.86
0.82
0.78
0.74
0.70
μ_A
0
1
2
3
β
30g 60g
2-3mm
1-2mm
0.5-1mm

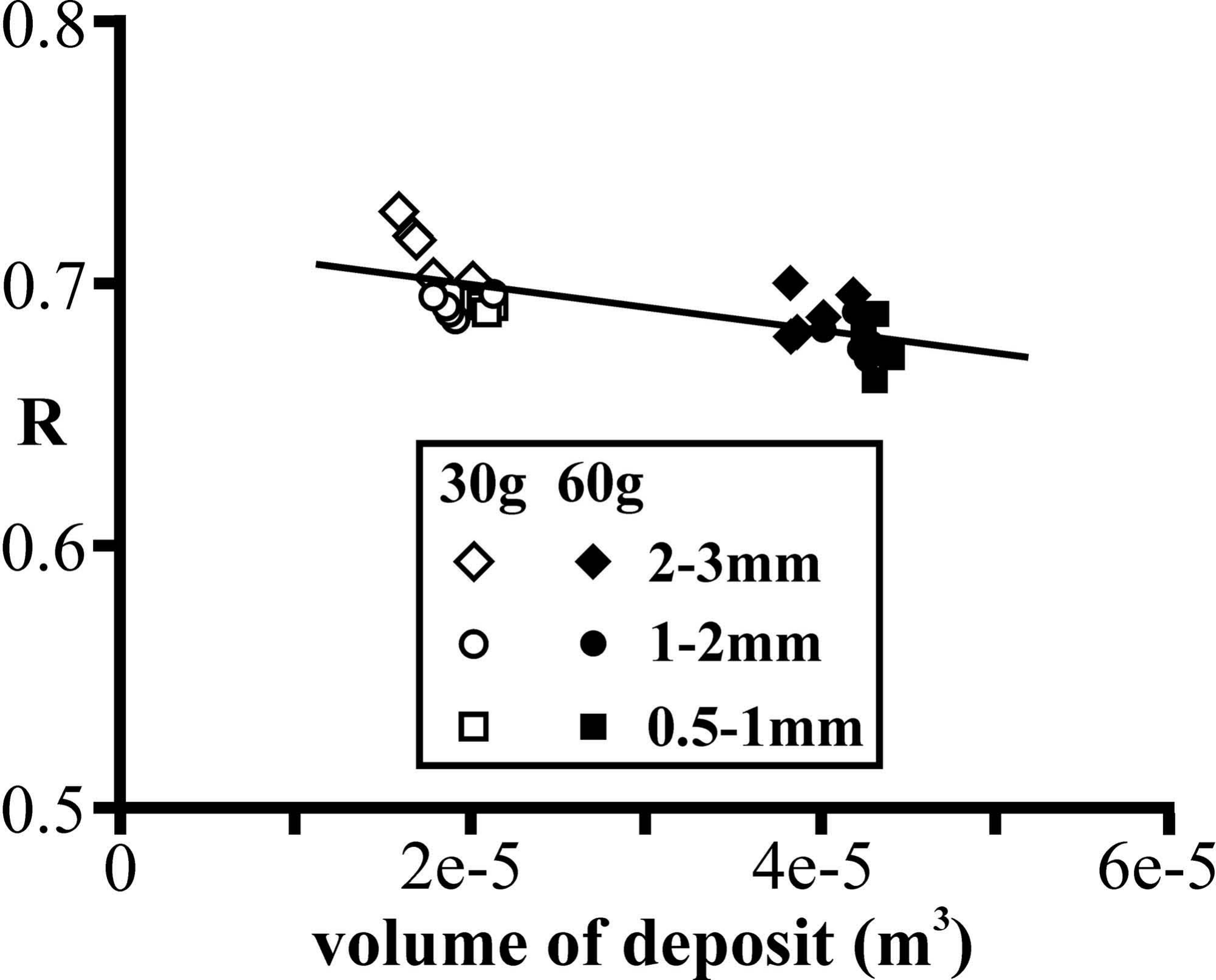
0.8
0.7
0.6
0.5
R
30g 60g
2-3mm
1-2mm
0.5-1mm
0
2e-5
4e-5
6e-5
volume of deposit (m3)

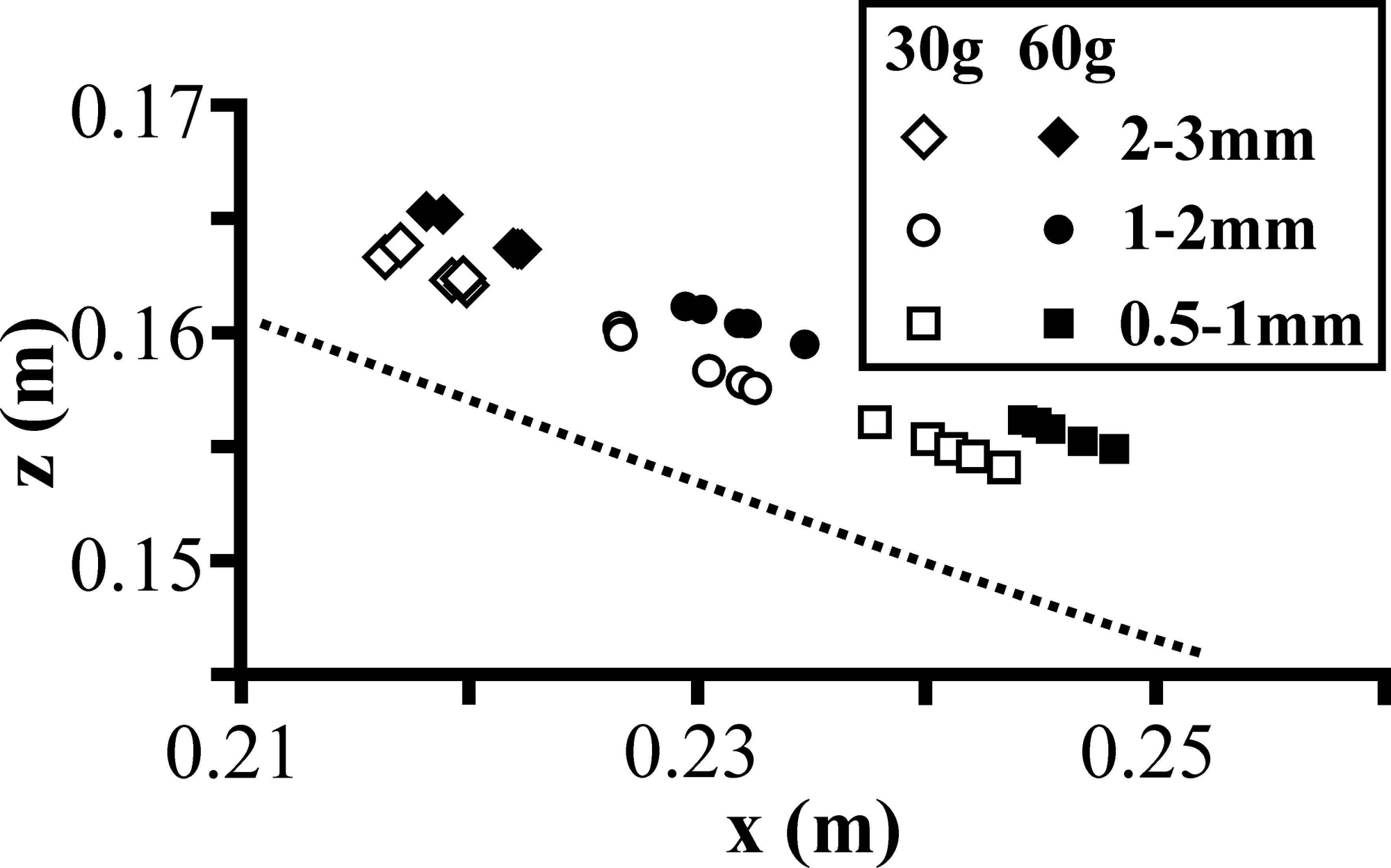
30g 60g
2-3mm
1-2mm
0.5-1mm
0.17
0.16
0.15
z (m)
0.21
0.23
0.25
x (m)